



## Article

# Dynamic Change Characteristics and Main Controlling Factors of Pore Gas and Water in Tight Reservoir of Yan'an Gas Field in Ordos Basin

Yongping Wan <sup>1</sup>, Zhenchuan Wang <sup>1</sup>, Meng Wang <sup>1</sup>, Xiaoyan Mu <sup>2</sup>, Jie Huang <sup>2</sup> , Mengxia Huo <sup>2</sup>, Ye Wang <sup>2</sup>, Kouqi Liu <sup>3</sup> and Shuangbiao Han <sup>2,\*</sup> 

<sup>1</sup> Gasfield Company of Shaanxi Yanchang Petroleum Group Co., Ltd., Yan'an 716000, China; wanhunter@163.com (Y.W.); 15289219955@163.com (Z.W.); wangmeng363x@163.com (M.W.)

<sup>2</sup> College of Geoscience and Surveying Engineering, China University of Mining and Technology, Beijing 100083, China; 18510912366@163.com (X.M.); lukehuangjie@163.com (J.H.); hmx06211908@163.com (M.H.); wy081520@163.com (Y.W.)

<sup>3</sup> Institute of Energy, Peking University, Beijing 100871, China; kouqi.liu@pku.edu.cn

\* Correspondence: hans@cumtb.edu.cn; Tel.: +86-134-2627-9176

**Abstract:** Tight sandstone gas has become an important field of natural gas development in China. The tight sandstone gas resources of Yan'an gas field in Ordos Basin have made great progress. However, due to the complex gas–water relationship, its exploration and development have been seriously restricted. The occurrence state of water molecules in tight reservoirs, the dynamic change characteristics of gas–water two-phase seepage and its main controlling factors are still unclear. In this paper, the water-occurrence state, gas–water two-phase fluid distribution and dynamic change characteristics of different types of tight reservoir rock samples in Yan'an gas field were studied by means of water vapor isothermal adsorption experiment and nuclear magnetic resonance methane flooding experiment, and the main controlling factors were discussed. The results show that water molecules in different types of tight reservoirs mainly occur in clay minerals and their main participation is in the formation of fractured and parallel plate pores. The adsorption characteristics of water molecules conform to the Dent model; that is, the adsorption is divided into single-layer adsorption, multi-layer adsorption and capillary condensation. In mudstone, limestone and fine sandstone, water mainly occurs in small-sized pores with a diameter of 0.001  $\mu\text{m}$ –0.1  $\mu\text{m}$ . The dynamic change characteristics of gas and water are not obvious and no longer change under 7 MPa displacement pressure, and the gas saturation is low. The gas–water dynamic change characteristics of conglomerate and medium-coarse sandstone are obvious and no longer change under 9 MPa displacement pressure. The gas saturation is high, and the water molecules mainly exist in large-sized pores with a diameter of 0.1  $\mu\text{m}$ –10  $\mu\text{m}$ . The development of organic matter in tight reservoir mudstone is not conducive to the occurrence of water molecules. Clay minerals are the main reason for the high water saturation of different types of tight reservoir rocks. Tight rock reservoirs with large pore size and low clay mineral content are more conducive to natural gas migration and occurrence, which is conducive to tight sandstone gas accumulation.

**Keywords:** Yan'an gas field; tight reservoir; gas–water distribution; nuclear magnetic resonance; absorption of water vapor; water saturation



**Citation:** Wan, Y.; Wang, Z.; Wang, M.; Mu, X.; Huang, J.; Huo, M.; Wang, Y.; Liu, K.; Han, S. Dynamic Change Characteristics and Main Controlling Factors of Pore Gas and Water in Tight Reservoir of Yan'an Gas Field in Ordos Basin. *Processes* **2024**, *12*, 1504. <https://doi.org/10.3390/pr12071504>

Academic Editor: Qingbang Meng

Received: 13 June 2024

Revised: 5 July 2024

Accepted: 11 July 2024

Published: 17 July 2024



**Copyright:** © 2024 by the authors. Licensee MDPI, Basel, Switzerland. This article is an open access article distributed under the terms and conditions of the Creative Commons Attribution (CC BY) license (<https://creativecommons.org/licenses/by/4.0/>).

## 1. Introduction

With the continuous development of the global economy, the demand for energy is increasing. The current tense energy situation is the background and premise for the development of unconventional oil and gas such as tight oil and gas [1]. A tight sandstone gas reservoir is a kind of valuable unconventional gas reservoir. According to statistics, the number of basins in the world where tight sandstone gas reservoirs are developed has exceeded 70 [2,3], making this category one of the largest unconventional gas reservoirs

in the world. Tight sandstone gas reservoirs are widely distributed in Ordos, Sichuan, Songliao, Tuha and other sedimentary basins in China. According to the results of the fourth oil and gas resource evaluation of PetroChina, the total resources of tight sandstone gas onshore in China have reached  $21.85 \times 10^{12} \text{ m}^3$ . The Upper Paleozoic of the Ordos Basin has reached  $13.32 \times 10^{12} \text{ m}^3$ , accounting for more than 60% of the total resources [4–6]. Shaanxi Yanchang Petroleum (Group) Co., Ltd., Yan'an City, China has carried out key exploration on the regional geological conditions of the Ordos Basin, reconstructed the Upper Paleozoic sedimentary model, and established the model of 'frequent migration of shallow water environment shoreline sand control' [7], which proves that the Ordos tight sandstone gas reservoir has broad exploration and development prospects.

The Ordos Basin is the absolute main battlefield for the exploration and development of tight sandstone gas in China. Since the 1990s, Jingbian, Sulige, Yulin, Zizhou, Daniudi and other gas fields have been discovered in the hinterland of the basin, and one after another exploration breakthroughs have been made. Formation water has a close influence on the formation, migration and occurrence of natural gas [8–10]. The relationship between oil, gas and water is one of the key factors determining oil and gas production in oil and gas exploration and development [1,11,12]. Previous studies have been carried out in the Ordos Basin. Many domestic scholars believe that there are multiple gas-bearing systems in the tight sandstone of the Upper Paleozoic in the Ordos Basin. Although the gas–water relationship is complex and there is no unified gas–water interface, there is no obvious gas–water inversion [13–16] Chen Chaobing found that the tight sandstone gas reservoirs in the northeastern Ordos Basin formed a pattern of "multi-layer gas-bearing, generally low-yield, and gas-water co-production" [8]. Cong Peng established two natural gas-accumulation models of "gas-water distribution controlled by source-reservoir configuration and physical property difference" and "gas-water distribution controlled by low-amplitude structure" in the low-mature gas area of Upper Paleozoic coal measures in the northeast of Yishan slope, Ordos Basin [17]. However, in recent years, with the large-scale exploration and development of tight sandstone gas, the phenomenon of water production in gas wells has made the production of tight sandstone gas very unstable [18,19]. To solve such problems, it is necessary to further clarify the gas–water dynamic relationship of tight reservoirs. However, scholars' understanding of the occurrence state of water, gas–water two-phase seepage characteristics and their influencing factors in tight gas reservoirs in Yan'an gas field is not mature. As a result, the exploration and development of tight sandstone gas in Yan'an gas field is hindered, so it is of great practical significance to clarify the gas–water distribution of tight gas reservoirs, clarify the dynamic change law of gas–water and the main controlling factors.

Nowadays, few scholars are conducting clear research on the dynamic relationship between gas and water in the tight reservoir of Yan'an gas field in Ordos. Based on the study of the basic characteristics of tight reservoirs in Yan'an gas field of Ordos Basin, this paper quantitatively characterized and analyzed the water molecular adsorption characteristics, gas–water two-phase fluid migration and occurrence dynamic changes of different types of tight reservoirs in Yan'an gas field by using water vapor isothermal adsorption experiments and nuclear magnetic resonance methane flooding experiments, and discusses the main controlling factors in combination with mineral, pore and organic geochemical characteristics. The results have certain reference value for further exploration and development of Yan'an gas field.

## 2. Geological Background and Samples

### 2.1. Geological Background

The Ordos Basin is a simple, ancient and stable multi-cycle basin in the northwest of China. Yan'an gas field is located in the southeastern part of the Yishan slope of the Ordos Basin (Figure 1). The Upper Paleozoic Carboniferous-Permian sedimentary development has experienced marine, marine–continental transitional and continental sedimentary system evolution, incomplete development and lack of Devonian and Lower Carboniferous strata. From bottom to top, it is divided into Upper Carboniferous Benxi Formation,

Lower Permian Taiyuan Formation and Shanxi Formation, Middle Permian Lower Shihezi Formation and Upper Shihezi Formation. The distribution range of the Carboniferous Benxi Formation-Permian Shanxi Formation 2 is wide, and the alternating conversion of sandstone, mudstone, coal and limestone is presented in the vertical direction, which provides a huge reservoir space for natural gas accumulation [20–22]. Yan’an gas field is far away from the northern source area, at the end of the sedimentary system, and the reservoir heterogeneity is stronger [23–25]. The distribution of gas fields is relatively scattered, showing the form of gas field groups [26]. Compared with the gas fields in the northern part of the basin, the geological conditions of the gas reservoirs are more complex, including more types of reservoir development [27].

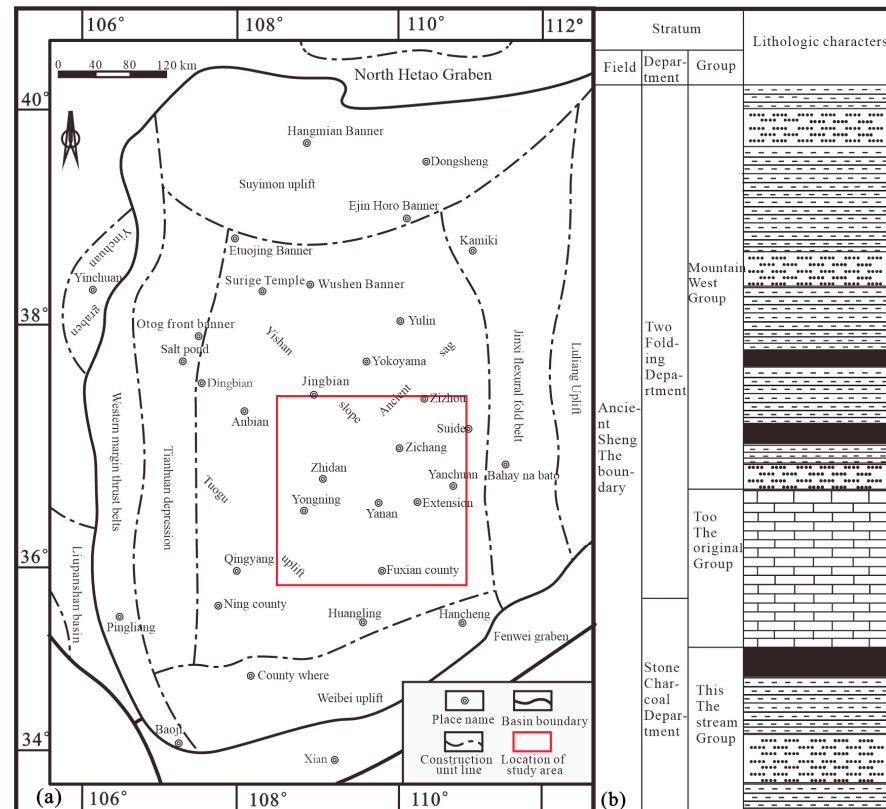


**Figure 1.** Structural location and stratigraphic conditions in the study area (Modified according to literature [28]). (a) The geological situation of Ordos Basin and the location of Yan’an gas field research area. (b) Stratigraphic and lithologic histogram of Ordos Basin.

Drilling data show that the main gas-producing horizons of Yan’an gas field are Benxi Formation to Shihezi Formation, and various rock types are developed in the reservoir. It is found that Benxi Formation and Shanxi Formation are the main source rock strata, mainly composed of gray-black mudstone and black coal seam. The coal seam is thinner than the mudstone, and the two are interlaced with each other, belonging to the marine–continental transitional facies sedimentary system. The total organic carbon (TOC) content of the source rock is high, the thermal evolution stage of the organic matter has reached the over-mature stage, and the vitrinite reflectance value is mostly in the gas-generation stage, which is the source of gas production in the sedimentary layer. Sandstone, limestone and conglomerate with different thicknesses are developed in the upper and lower layers of source rocks, which are the main storage sites of natural gas.

## 2.2. Samples

In this study, a total of 15 different types of tight reservoir samples were selected from mudstone, sandstone, conglomerate and limestone samples of the Upper Paleozoic Shanxi

Formation, Benxi Formation, Taiyuan Formation and Shihezi Formation in different regions of Yan'an gas field. The basic information of the samples is shown in Figure 2 and Table 1.

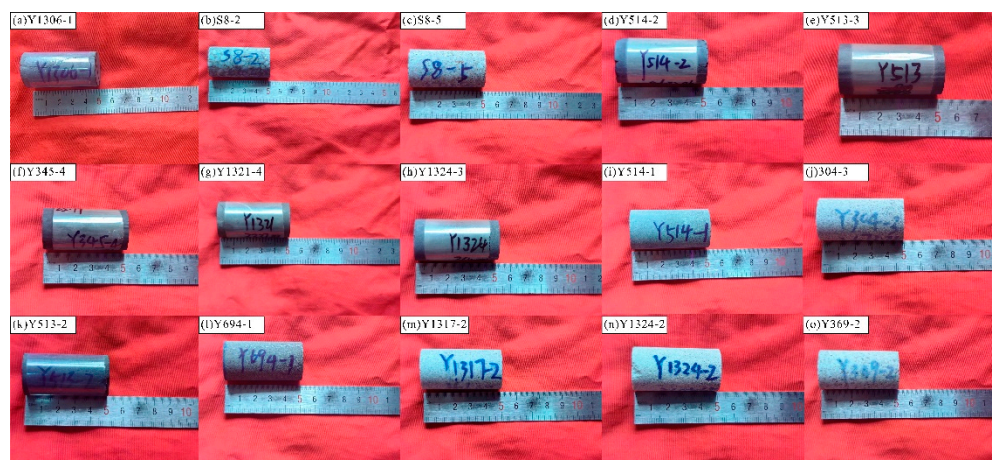


**Figure 2.** The picture of Yan'an gas field samples.

The average TOC and hydrocarbon-generation potential (S1 + S2) of mudstone samples are 1.284% and 0.39 mg/g, the type index (S2/S3) is less than 3, the average vitrinite reflectance and maximum pyrolysis temperature (Tmax) are 2.502% and 444.2 °C, indicating that the organic matter abundance of mudstone samples is medium to high, the organic matter type is mainly type III humic type, and it is in the high over mature stage. The mineral content of different types of tight reservoir rock samples in Yan'an gas field varies greatly (Figure 3a). The average content of quartz in sandstone is 68.5%, followed by clay mineral content, with an average content of 27.8%, and feldspar mineral development is less, with an average of 2.3%. The main mineral of conglomerate is quartz, with an average of 92%, and limestone is completely composed of calcite minerals. The calcite content of the Y345-4 sample is the highest, reaching 40.9%, while the siderite content of the Y1321-4 sample is higher, reaching 60.7%. The mineral composition of these two samples is special, which has certain comparative reference significance for the study of gas–water distribution characteristics in microscopic pores of mudstone. The remaining mudstone mineral content is dominated by quartz and clay minerals, with an average of 53.67% for quartz and 38.8% for clay minerals. The clay minerals of mudstone are mainly illite, with an average content of 50%, followed by kaolinite and illite, with an average content of 28.25% and 29.33%, respectively.

The pore volume of 0–2 nm micropores in mudstone samples is mainly provided by 0.45–0.95 nm pores. The average pore size of source rocks is 0.8146 nm, the average specific surface area is 5.675 m<sup>2</sup>/g and the average total pore volume is 0.0021 cm<sup>3</sup>/g by density functional theory (DFT) simulation. The pore structure parameters of different types of tight reservoir rock samples in Yan'an gas field are shown in Table 1, and the pore structure characteristics are quite different (Figures 4 and 5). The results of low-temperature nitrogen-adsorption experiments show that the 2–50 nm mesoporous pore morphology types are mainly parallel plate pores and fractured pores. The conglomerate and Y304-3 sandstone samples also have some ink bottle pore characteristics, mainly due to their similar mineral composition, and all of them are Benxi Formation rock samples. The 2–50 nm mesoporous pore volume of most samples is mainly provided by about 4 nm pores. The smaller pores of Y1321-4, Y1306-1, conglomerate and Y304-3 samples provide the larger pore volume. The pore volume of Y1321-4 and Y1306-1 is provided by 2–4 nm pores, while the pore volume of conglomerate and Y304-3 is provided by 2 nm pores. The high-pressure mercury-injection experiment shows that the pore connectivity of different types of tight reservoir rock samples in Yan'an gas field is quite different, and the pore connectivity of mudstone and limestone samples is stronger than that of sandstone and conglomerate. The displacement pressure of limestone and most sandstone and mudstone samples is about 5–10 MPa, and the pore volume is mainly provided by 7–2000 nm pores. The smaller the pore size, the larger the pore volume.



**Table 1.** Basic information of tight reservoir in Yan'an gas field.

Sample Number	Depth (m)	Stratum	Lithology	Low Temperature N <sub>2</sub> Adsorption			High Pressure Mercury Intrusion				
				Specific Surface Area (m <sup>2</sup> /g)	Total Pore Volume (cm <sup>3</sup> /g)	Average Pore Size (nm)	Pore Volume (cm <sup>3</sup> /g)	Permeability (10 <sup>-3</sup> μm <sup>2</sup> )	Porosity (%)	Mercury Withdrawal Efficiency (%)	Displacement Pressure (MPa)
Y1306-1	3420.71	Taiyuan Formation	Limestone	0.683	0.0026	15.28	0.0029	0.0004	0.73	74.38	5.50
S8-2	2706.26	Benxi Formation	Gray-white medium conglomerate	0.239	0.0010	17.32	0.0137	0.2990	3.58	40.62	0.47
S8-5	2723.98	Benxi Formation	Gray-white coarse conglomerate	0.183	0.0008	18.03	0.0100	0.8740	2.66	36.39	0.26
Y514-2	2622.06	Shanxi Formation	Grayish black mudstone	5.146	0.0156	12.16	0.0029	0.0066	0.77	80.21	0.67
Y513-3	2718.77	Shanxi Formation	Grayish black mudstone	2.730	0.0089	13.07	0.0039	0.0001	1.03	82.15	13.78
Y345-4	2725.79	Benxi Formation	Grayish black mudstone	3.018	0.0090	11.94	0.0013	0.0063	0.42	59.01	0.67
Y1321-4	3337.83	Benxi Formation	Black gray mudstone	0.701	0.0024	13.50	0.0013	0.0002	0.48	60.37	5.51
Y1324-3	3640.41	Shanxi Formation	Dark gray mudstone	5.951	0.0176	11.84	0.0030	0.0001	0.84	71.80	13.77
Y514-1	2524.57	Shihezi Formation	Light gray fine sandstone	2.605	0.0090	13.85	0.0081	0.0105	2.18	41.07	0.67
Y304-3	2673.76	Benxi Formation	Light gray fine sandstone	1.632	0.0009	2.21	0.0273	1.9380	6.74	35.94	0.26
Y513-2	2687.57	Shihezi Formation	Light gray fine sandstone	2.914	0.0099	13.61	0.0050	0.0002	1.30	56.28	13.78
Y694-1	3257.18	Shihezi Formation	Gray fine sandstone	1.805	0.0063	14.05	0.0088	0.0090	2.29	46.48	0.67
Y1317-2	3361.69	Shanxi Formation	Gray-white medium sandstone	1.393	0.0044	12.62	0.0100	0.0613	2.60	52.29	0.67
Y1324-2	3605.55	Shihezi Formation	Light gray medium sandstone	2.526	0.0090	14.30	0.0387	0.4530	9.40	45.20	0.47
Y369-2	3018.86	Shanxi Formation	Gray-white pebbly coarse sandstone	0.637	0.0020	12.70	0.0121	0.1880	3.10	60.33	0.47

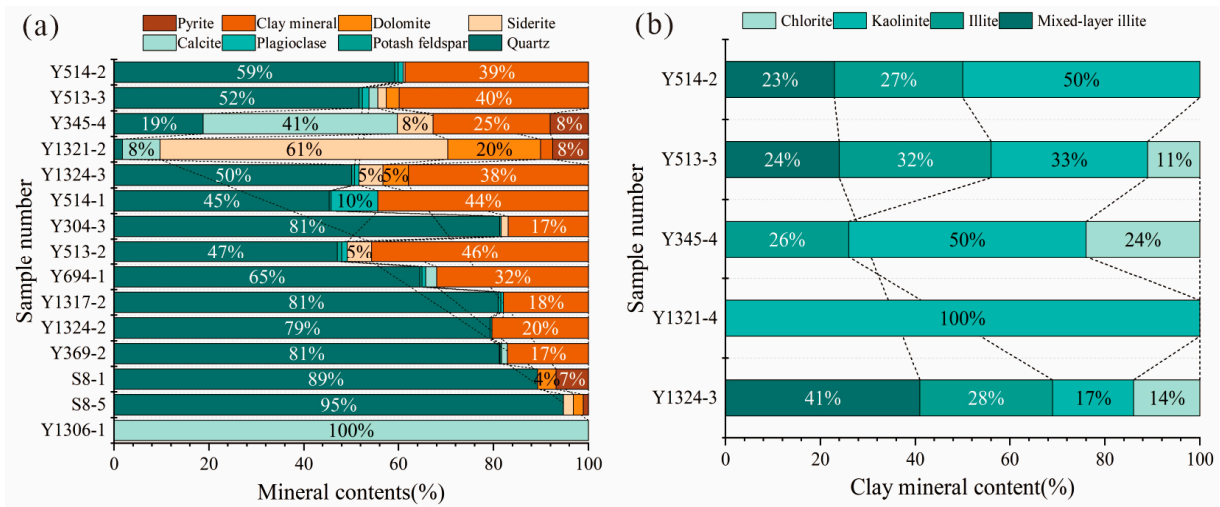


**Figure 3.** Mineral content of tight reservoir and clay mineral content of mudstone in Yan'an gas field. (a) Relative content of different types of minerals in rocks. (b) Relative content of each component of clay minerals.

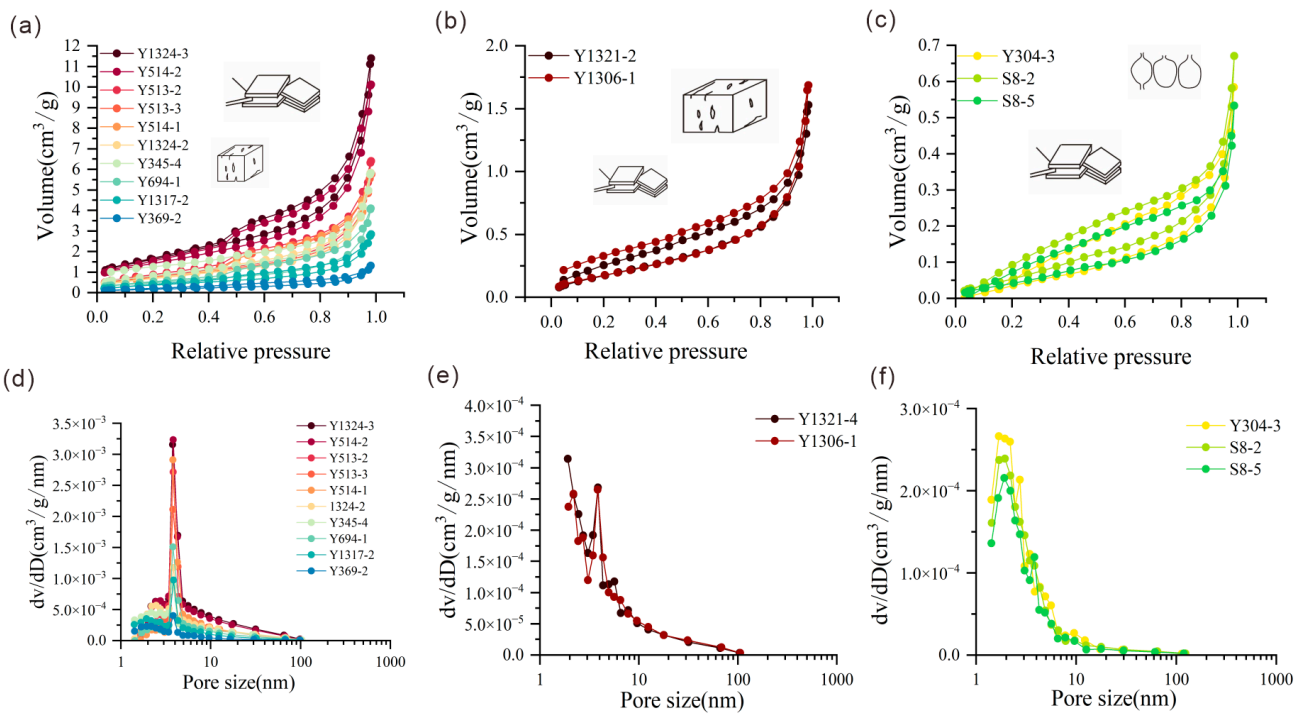


**Figure 4.** Low temperature nitrogen adsorption-desorption curve and pore size distribution of tight reservoir in Yan'an gas field. (a-c) Low temperature nitrogen adsorption-desorption curve of 15 rock samples from Yan'an gas field. (d-f) Pore size distribution of 15 tight reservoir rock samples in Yan'an gas field based on low temperature nitrogen adsorption experiment.

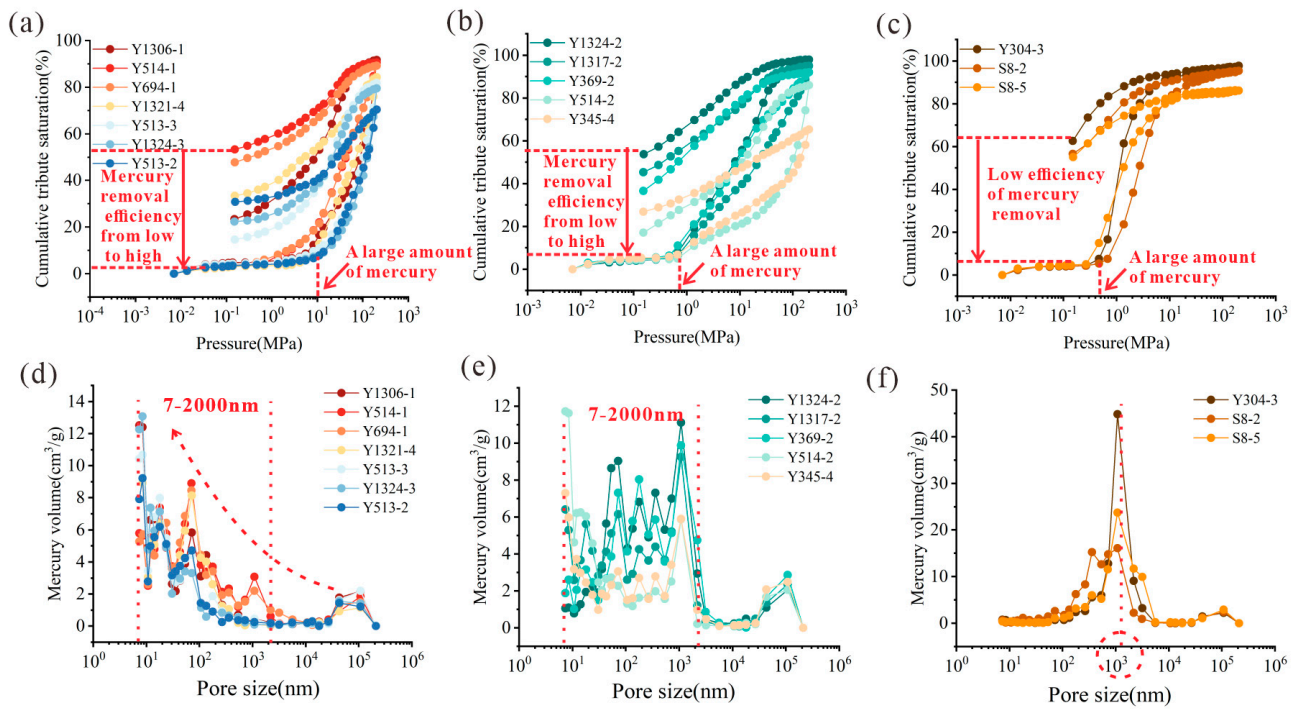


**Figure 5.** High pressure mercury injection curve and pore size distribution of tight reservoir in Yan'an gas field. (a–c) High pressure mercury intrusion-mercury withdrawal curve of 15 rock samples from Yan'an gas field. (d–f) Pore size distribution of 15 tight reservoir rock samples in Yan'an gas field based on high-pressure mercury intrusion experiment.

### 3. Experimental Methods

#### 3.1. Water Vapor-Adsorption Experiment and Adsorption Kinetics Model

The water vapor-adsorption experiment was completed with the BESTD multi-station gravimetric gas vapor adsorption instrument (BSD-VVS). Before the water vapor-adsorption experiment, it is necessary to crush different types of tight reservoir samples to 60~80 mesh, and uniformly select 500 mg powder samples for the experiment. The experimental test temperature is 25 °C, the test relative pressure range is 0–1 and the adsorption equilibrium condition is 0.1 mg/60 min. The experimental steps are as follows: ① the sample is placed in the sample tube of the adsorber, and the sample is degassed at 150 °C for 3 h by heating vacuum degassing to remove water, air and other impurity gases in the sample until the sample quality is constant; ② set the experimental temperature to 25 °C; ③ the mass of the sample tube at different time points and different relative pressures was obtained by microbalance, so as to obtain the water vapor adsorption and desorption curve of the sample.

In order to deeply understand the microscopic mechanism of water molecule adsorption by different types of tight reservoir rocks in Yan'an gas field, this study selected the Langmuir model, Freundlich model, DW model, DS2 model, GAB model and Dent model to fit the water vapor isothermal adsorption curve of the samples. Based on this, the appropriate theoretical model was selected to process the experimental data to extract meaningful adsorption characteristic parameters for quantitative comparative analysis by comparing the applicability of the six models for rock adsorption. (Table 2).

**Table 2.** Adsorption kinetics fitting model of water vapor-adsorption experiment.

Name of Fitting Model	Mathematical Expression	Remark
Langmuir [29]	$q = q_0 \frac{k_1 h}{1 + k_1 h}$	$q$ : Adsorption water, mg/g; $q_0$ : The maximum adsorbed water amount of single molecular layer, mg/g; $k_1$ : Langmuir constant, dimensionless; $h$ : Relative pressure, dimensionless.
Freundlich [30,31]	$q = q_0 (h)^{\frac{1}{n}}$	$n$ : Strength between adsorbent and adsorbate.
DS2 [32,33]	$q = (q_0 + q)(1 - k_2 q)h$	$k_2$ : The adsorption constant related to the degree of reduction of the secondary adsorption sites, dimensionless.
DW [34,35]	$q = \frac{q_0 k_1 h}{1 + k_1 h} + \frac{q_1 k_2 h}{1 - k_2 h}$	$q_1$ : The amount of adsorbed water at the first adsorption point, mg/g.
GAB [36–38]	$q = \frac{q_0 C k h}{(1 - k h)(1 + (C - 1) k h)}$	$C$ : The size of the value can reflect the speed of the formation of multi-molecular layers. $k$ : Adsorption constant related to adsorption energy, dimensionless.
Dent [34,36–38]	$q = \frac{q_0 K h}{(1 - k h)(1 + K h - k h)}$	$K = Ck$ ; $K$ : Adsorption constant related to adsorption energy, dimensionless.

### 3.2. Nuclear Magnetic Resonance Methane Flooding Experiment

The nuclear magnetic resonance methane flooding experiment was completed with a Suzhou Newmai Mesomr12-150H-I large aperture nuclear magnetic resonance analyzer. Before the water vapor-adsorption experiment, the plunger samples of different types of tight reservoir samples need to be prepared. The sample size was 25 mm in diameter and 4–5 mm in length. In order to be able to carry out a unified comparative analysis of different types of tight reservoir rock samples, after considering the properties and characteristics of the samples, the experimental test conditions were set to 25 °C experimental test temperature, 20 MPa vacuum pressure saturated water pressure and 15 MPa maximum gas drive pressure. The experimental steps are as follows: ① The sample was dried in a blast drying oven, dried to the constant weight of the sample and the dry weight of the sample was tested. ② In order to make the core completely saturated with water at 20 MPa, the mass and volume of the sample saturated with water were tested. The sample was subjected to pressurized saturated water treatment at 20 MPa for 24 h. ③ The pressurized saturated samples were loaded into a high-temperature and high-pressure non-magnetic core holder with a facility confining pressure of 20 MPa to test the nuclear magnetic resonance  $T_2$  spectrum signal of saturated water samples. ④ The gradient pressure displacement was carried out according to the test purpose. The test pressure points were 1 MPa, 2 MPa, 3 MPa, 5 MPa, 7 MPa, 9 MPa, 12 MPa and 15 MPa, respectively. Each pressure point needs to be tested repeatedly until the  $T_2$  spectrum does not change, and the final quality of the sample is recorded. ⑤ According to the  $T_2$  spectrum data obtained under different gas drive pressures, the porosity, gas drive water efficiency, water (gas) saturation and other parameters of the core can be calculated.

### 3.3. Other Experimental

The TOC of mudstone samples was determined by Leco SC-632 according to Chinese GB/T 19145-2022 standard [39], Ro was tested with a microscope photometer, and rock pyrolysis experiment was carried out with the Rock-Eval 6 instrument according to Chinese GB/T 18602-2012 standard [40]. According to Chinese SY/T 5163-2018 [41], the whole rock and mudstone clay minerals of all samples were analyzed with a Bruker AXS D8 Discover X-ray diffractometer. According to Chinese GB/T 21650.2-2008/ISO 15901-2:2006 and



Chinese GB/T 21650.3-2011/ISO 15901-3:2007 [42,43], the low temperature carbon dioxide-adsorption and -desorption experiments of mudstone samples and nitrogen-adsorption and -desorption experiments of all samples were completed by using a Quantachrome NOVA specific surface and pore size-distribution analyzer. According to Chinese GB/T 21650.1-2008/ISO 15901-1:2005 [44], the samples were tested with an AutoPore IV 9505 automatic mercury porosimeter.

#### 4. Isothermal Adsorption Characteristics of Water Vapor

##### 4.1. Water Vapor Adsorption–Desorption Curve

Figure 6 shows the isothermal adsorption–desorption curves of 15 rock samples in this experiment. It can be seen that with the increase in relative pressure, the water vapor content of rock samples increases gradually, but there are significant differences in the water vapor-adsorption capacity of different types and different rock samples of the same type. Among them, the maximum adsorption capacity of water vapor in mudstone samples can reach 19.15 mg/g, and the minimum value is only 2.17 mg/g; the maximum water vapor-adsorption capacity of the sandstone sample is 18.47 mg/g, and the low value is only 2.91 mg/g. The adsorption capacity of other rocks is about 2.0 mg/g. The International Union of Pure and Applied Chemistry (IUPAC) divides the isothermal adsorption curve into types I–VI [45]. After observation and analysis, the isothermal adsorption curve of mudstone samples in this study conforms to the characteristics of the type II isothermal adsorption line. In the early stage, with the increase in relative pressure, multi-layer adsorption gradually formed. When the saturated vapor pressure was reached, the adsorption layer was infinite, resulting in a significant increase in adsorption capacity. Although the isothermal adsorption curve of tight glutenite samples has different inflection points and degrees, the overall shape is ‘S’ type, which also belongs to the type II curve [46]. If the isothermal adsorption curve does not coincide with the desorption curve, it indicates that the desorption is incomplete, and the part separated from the two curves is the hysteresis loop. IUPAC divided the hysteresis loop into H1–H5 types in 2015 [45]. After observation and analysis, the hysteresis loops of the samples in this study were mainly H2–H3 type, H3 type and H3–H4 type, indicating that the samples developed flat a slit structure, cracks, a wedge structure and narrow fracture pores, and there may be micropore filling and ink bottle-shaped pores.

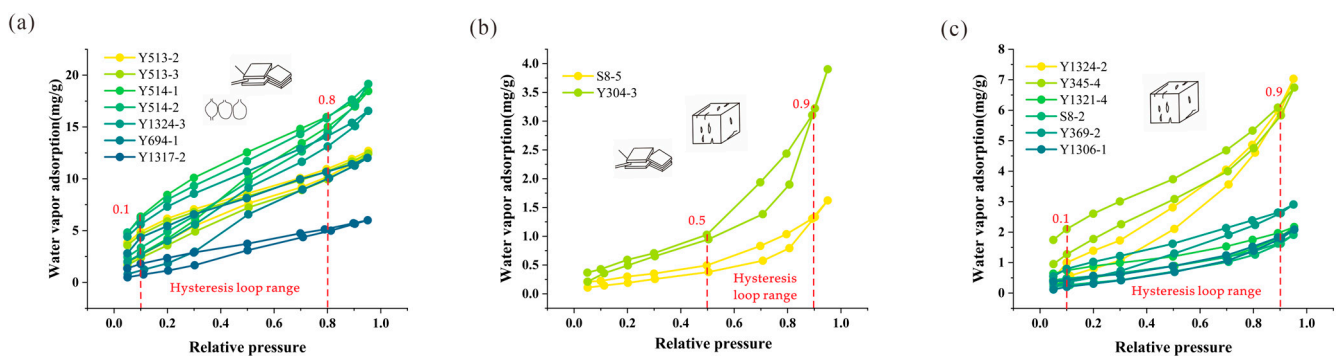


**Figure 6.** Water vapor adsorption–desorption curve. (a) Water vapor adsorption–desorption curves of 7 Yan’an gas field rock samples. (b) Water vapor adsorption–desorption curves of 2 Yan’an gas field rock samples. (c) Water vapor adsorption–desorption curves of 6 Yan’an gas field rock samples.

According to the size and morphological characteristics of the water vapor hysteresis loop, 15 samples were initially divided into three categories: ① Figure 6a: The water vapor isothermal adsorption–desorption curve of this type of sample is mainly H2–H3 type, which lags significantly in the 0.0–0.8 relative pressure section, and the desorption curve is not closed. ② Figure 6b: This type of sample water vapor isothermal adsorption–desorption curve is H3 type, in the 0.5–0.9 relative pressure section lag; the closure characteristics

of desorption curve are more obvious than 1. ③ Figure 6c: The water vapor isothermal adsorption–desorption curve of this type of sample is mainly H3-H4 type, which lags behind in the 0.1–0.9 relative pressure section, and the unclosed characteristic of the middle-low desorption curve is not obvious compared with type ①. The type ① water vapor-like hysteresis loop is more obvious at medium-low pressure. Generally, the formation of a hysteresis loop is mainly affected by capillary condensation and occurs in the middle-high relative pressure section [47], indicating that ① the adsorption–desorption of water vapor is affected by more complex factors. In previous studies, it was found that there may be the following reasons: with the increase in relative pressure, only a small amount of water molecules are adsorbed at the polar site at a lower relative pressure, and hydrogen bond molecular clusters are formed around the first adsorption site. Molecular groups combine to fill pores and fissures [48]; micropore filling leads to clay expansion and deformation, which narrows the micropore channel and leads to a hysteresis loop under low relative pressure [48–50]. The hysteresis loop may be related to the combination of strongly hydrophilic quartz with water molecules at low relative pressure. The type ② hysteresis loop belongs to H3 type. When  $P/P_0 = 0.5$ , the hysteresis begins to be close to adsorption, and the hysteresis loop appears in the high-medium pressure section, which may be related to capillary condensation and the ink bottle pore effect [51,52]. The hysteresis adsorption at high relative pressure may be divided into single-layer adsorption, multi-layer adsorption and finally capillary condensation with increased relative pressure [34]. The type ③ hysteresis loop is H3-H4 type. Among them, the desorption hysteresis of Y345-4 at the lowest  $P/P_0$  basically coincides with the adsorption, and the other samples show the characteristics of type ① non-closure.

#### 4.2. Thermodynamic Model Fitting of Water Vapor Adsorption

The fitting results of the model are shown in Table 3 and Figure 7.

**Table 3.** Adsorption curve-fitting parameters of rock samples in Yan’an gas field.

Sample Number	Fitted Model	Freundlich			DS2			Dent			
		$q_0$	$1/n$	$R^2$	$q_0$	$k_2$	$R^2$	$q_0$	$K$	$k$	$R^2$
Y513-3		12.227	1.320	0.991	13.042	2.129	0.955	6.338	5.205	0.555	0.997
Y514-2		18.496	1.161	0.978	19.176	0.363	0.969	7.485	6.702	0.659	0.997
Y345-4		6.233	1.165	0.942	6.468	1.150	0.934	2.034	14.143	0.736	0.998
Y1324-3		16.471	1.154	0.991	17.052	2.129	0.983	8.669	3.631	0.561	0.995
Y1321-4		1.998	1.021	0.924	2.008	0.232	0.924	0.560	16.964	0.782	0.999
Y369-2		2.952	0.876	0.992	2.851	0.709	0.986	1.522	2.001	0.601	0.998
Y1324-2		7.257	0.557	0.980	6.100	0.602	0.906	2.145	1.905	0.772	0.999
Y1317-2		6.274	0.962	0.997	6.213	2.100	0.997	11.346	0.524	0.259	0.997
Y513-2		12.405	1.433	0.990	13.460	1.151	0.925	6.570	6.115	0.540	0.996
Y514-1		18.731	1.111	1.092	19.220	3.174	0.991	12.999	2.121	0.465	0.995
Y304-3		4.224	0.359	0.917	3.044	0.685	0.788	0.552	10.955	0.909	0.993
Y1306-1		2.089	0.649	0.970	1.849	0.337	0.928	0.569	3.645	0.783	0.999
S8-2		1.837	0.785	0.947	1.721	0.453	0.932	0.465	8.780	0.803	0.997
S8-5		1.774	0.347	0.924	1.260	0.787	0.783	0.227	10.659	0.910	0.993

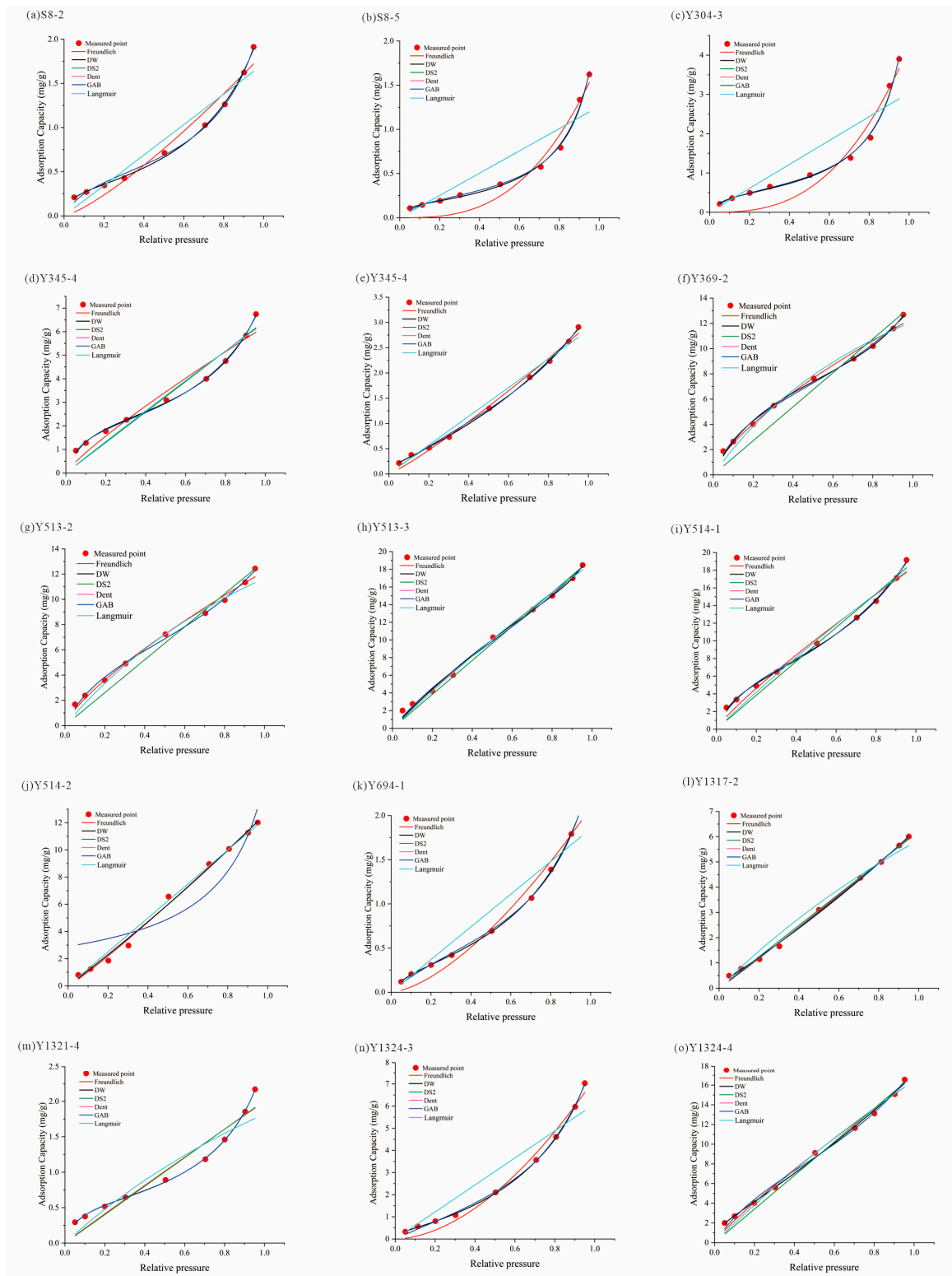


**Figure 7.** Fitting results of different fitting models.

The fitting results of the Langmuir model of the water vapor isothermal adsorption curve show that the fitting of nine rock samples is not convergent. Although the correlation coefficient of individual sample curve fitting is high, the fitting effect is not good in the whole relative pressure range, and the residual value is very large. This may be because the applicable condition of the Langmuir model is that the adsorption occurs on the isotropic

uniform adsorption surface, which is used to describe the monolayer adsorption [53]. In the actual situation, the mineral composition of the rock itself is very complex and cannot provide an isotropic uniform adsorption surface. In addition, multi-layer adsorption and capillary condensation of water vapor will occur under medium-high relative pressure conditions, and the Langmuir model is no longer applicable. The Freundlich model considers the heterogeneity of the adsorption sites and the surface heterogeneity of the pores and fractures, but it is mainly used for the adsorption behavior of the surface heterogeneity of clay minerals [32,54]. The samples in this experiment are mainly dense rock samples, and the clay content is not high, so the final fitting effect is general. The DS2 model considers the occupation effect of water molecule adsorption on the secondary adsorption site. The DS2 model considers that the adsorption of water vapor in activated carbon mainly occurs at the primary adsorption site such as oxygen-containing functional groups. The formula has been improved [33,55], but the properties of the rock samples in this experiment are quite different, and the fitting effect is not very good. The DW model assumes that there are two adsorption methods for water molecules: single molecular layer adsorption directly adsorbed on the surface of the adsorbent and multi-molecular layer adsorption adsorbed on the outer layer of the adsorbed water molecules [35,56]. The experimental results show that all the samples in this experiment have good fitting effect; except for the Y694-1 sample, all have  $R^2 > 0.995$ , but there are four parameters in this fitting method, and there is an over-fitting problem. GAB is a multi-layer adsorption model based on Langmuir theory, BET multi-molecular layer adsorption theory and kinetic theory of double adsorption point hypothesis. It can describe the single-layer and multi-layer adsorption process and most of the range. The fitting results are very suitable except for Y694-1, and can effectively define the single-layer and multi-layer adsorption. However, studies have shown that the GAB model cannot reflect the adsorption position of water vapor [53,57]. The Dent model and the GAB model have the same scope of application and formula theory. The adsorption process is divided into primary adsorption and secondary adsorption, covering two adsorption processes of molecular layer adsorption and capillary condensation [58,59]. The model fitting effect is  $R^2 > 0.992$  for all samples except Y694-1. Based on the above results and previous experience, this article selects the Dent model-fitting results for discussion.

## 5. Variation Characteristics of Nuclear Magnetic Resonance Methane Flooding

### 5.1. Occurrence Characteristics of Gas and Water in Pores

The area enclosed between the NMR  $T_2$  spectrum curve and the relaxation time ( $T_2$ ) horizontal axis of the core can represent the pore space of all the water in the core. The water saturation in the fully saturated water state is 100% [4,5], and the volume of water in the sample can be calculated. The porosity can be calculated by the ratio of water volume to sample volume.  $T_2$  relaxation time can be used to characterize the pore size of core samples. A short relaxation time corresponds to small pores, and a long relaxation time corresponds to large pores [6]. The  $T_2$  spectrum can be converted into a pore size-distribution map by calculating the surface relaxation rate. Due to the large differences in rock samples of different types of tight sandstone reservoirs, the surface relaxation rates of different rock samples were calculated by combining high-pressure mercury-injection experiments and nuclear magnetic resonance saturated  $T_2$  spectra, and the nuclear magnetic resonance  $T_2$  value was converted into pore diameter (Figure 8).



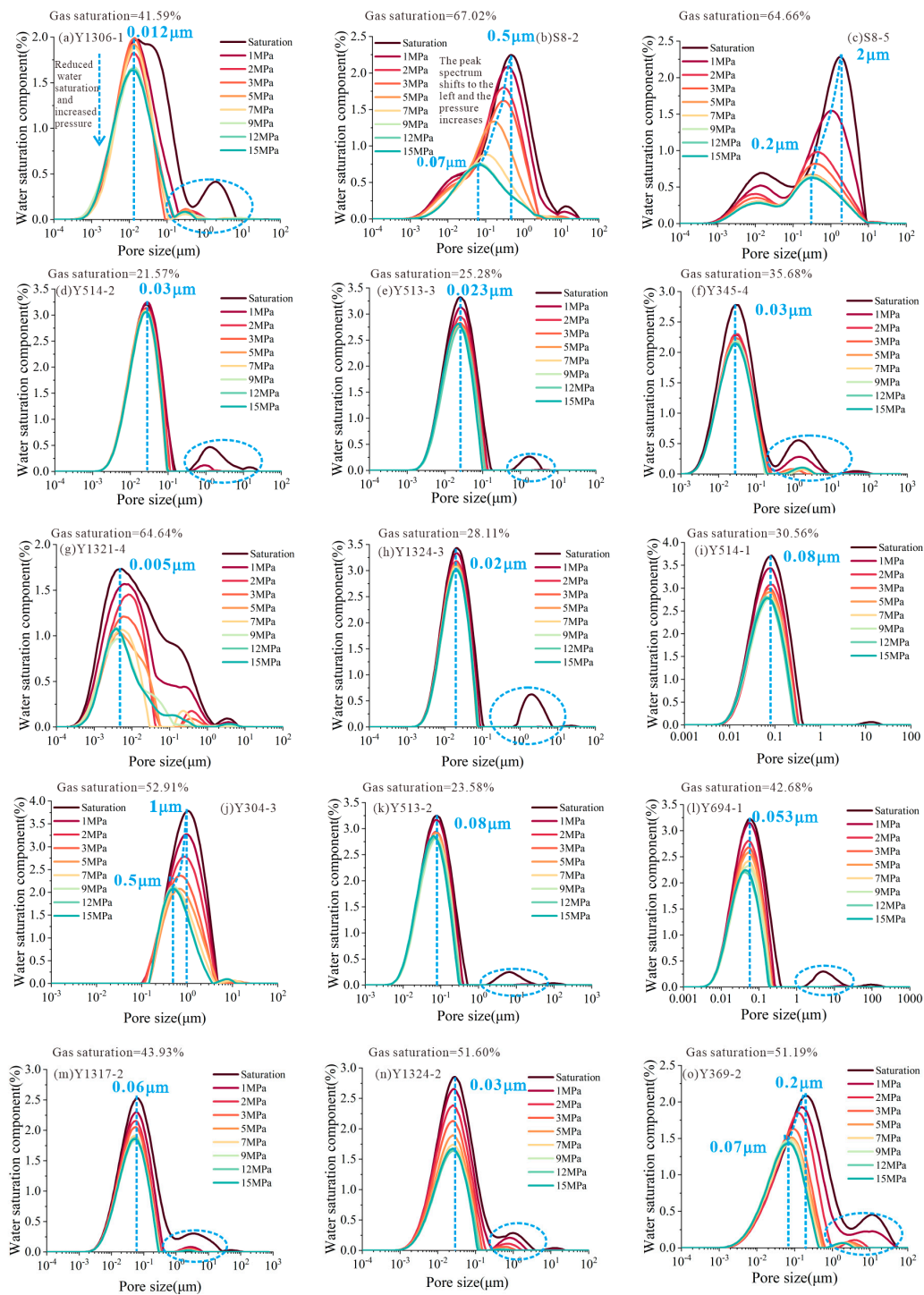


**Figure 8.** Change of water saturation. The dotted circle indicates that this pore sizes has a high degree of displacement effect.

As shown in Figure 8, the variation characteristics of water saturation in rock samples of different types of tight reservoirs are quite different. The area of the water saturation component curve of the nuclear magnetic resonance and the aperture is the water content of the corresponding aperture. The complete water-saturated state curves of most samples show bimodal characteristics. It is obvious that the area of short relaxation time of limestone, mudstone and sandstone samples is much larger than that of long relaxation time; that is, the water content of small size pores is significantly higher than that of large size pores.

The completely saturated state curves of the Y304-3 sample and conglomerate mainly show single peak characteristics. The area of the  $T_2$  spectrum curve and abscissa is mainly composed of large-sized pores, indicating that water mainly occurs in large-sized pores. The pore size of water saturation distribution of limestone and mudstone reservoirs (except Y1321-4) in Yan'an gas field is mainly between 0.001  $\mu\text{m}$  and 0.1  $\mu\text{m}$ , while that of fine sandstone reservoirs (except Y304-3) is mainly between 0.01  $\mu\text{m}$  and 0.1  $\mu\text{m}$ , and that of medium sandstone, coarse sandstone and conglomerate samples with larger particle size is mainly between 0.001  $\mu\text{m}$  and 10  $\mu\text{m}$ . The pore size-distribution characteristics of different types of tight reservoir rocks are calculated, which are consistent with the pore size-distribution characteristics obtained by low temperature carbon dioxide adsorption, low temperature nitrogen adsorption and high pressure mercury-injection experiments. The nuclear magnetic porosity, gas saturation and water saturation of different types of tight reservoirs are shown in Figure 8. The nuclear magnetic porosity and mercury intrusion porosity data show a very good correlation, indicating the accuracy of the nuclear magnetic resonance methane flooding experimental method. The porosity of limestone is only 0.43%, the NMR porosity of mudstone is relatively low (the average value is 1.66%) and the NMR porosity of sandstone and conglomerate is relatively high (the average values are 3.70% and 2.74%, respectively). However, in general, the NMR porosity of tight reservoirs in Yan'an gas field is low (the average value is 2.67%), showing a very obvious trend of decreasing porosity with the decrease in rock particle size.

### 5.2. Gas–Water Distribution Dynamic Change

With the increase in methane flooding pressure, the occurrence state of water in pore space, namely water saturation, will change (Figure 9), and the movable water content will decrease. The water still exists in the core under the maximum methane flooding pressure (15 MPa) and is bound water. The water in large-sized pores is preferentially expelled. For example, the water in 1–10  $\mu\text{m}$  pores in limestone, mudstone and fine sandstone is almost completely expelled, and the water in small-sized pores is slowly expelled with the increase in methane flooding pressure. The change of water saturation curve in limestone and mudstone (except Y1321-4) is small, and the change trend is the most obvious in the pores with pore diameter of 0.01–0.03  $\mu\text{m}$ , indicating that the water in the pores of this size is gradually expelled, and the gas saturation provided is larger. The change trend of the water saturation curve in conglomerate is the most obvious. For example, the peak position of the water saturation curve of the S8-2 sample gradually decreases from 0.5  $\mu\text{m}$  pore to 0.07  $\mu\text{m}$  pore, and a large range of pores provide a large amount of gas saturation. The change trend of water saturation in sandstone is stronger than that in mudstone and limestone, and weaker than that in conglomerate. The change of water saturation in different sandstone samples is also different. The change trend of water saturation in most sandstone samples is the most obvious in the pores with pore diameter of 0.05–0.08  $\mu\text{m}$ . The quartz mineral content of the Y304-3 sample is high. The pore size distribution and pore connectivity characteristics of nitrogen adsorption and high-pressure mercury-injection experiments are similar to those of conglomerate. The water saturation curve shows a single peak distribution, and the water saturation is mainly provided by large pores of 0.1  $\mu\text{m}$ –3  $\mu\text{m}$ . With the increase in methane flooding pressure, the peak position of the water saturation curve of the Y304-3 sample gradually decreases from 1  $\mu\text{m}$  pore to 0.5  $\mu\text{m}$  pore. The change of the water saturation curve of the Y369-2 sample with larger particle size is also similar to that of conglomerate and the Y304-3 sample, but the water saturation of this sample is mainly between 0.001  $\mu\text{m}$  and 10  $\mu\text{m}$ , and the distribution range is larger. With the increase in methane flooding pressure, the peak position of the water saturation curve of the Y304-3 sample gradually decreases from 0.2  $\mu\text{m}$  pore to 0.07  $\mu\text{m}$  pore.

As shown in Figure 9, the water saturation of rock samples in different types of tight reservoirs varies significantly with the pressure of methane flooding. The water saturation of mudstone and fine sandstone does not change significantly when the water pressure of methane flooding reaches about 7 MPa, while the water in mudstone and fine sandstone

mainly occurs in 0.001~0.01  $\mu\text{m}$  pores, and the main pore diameter of water saturation change is between 0.01 and ~0.08  $\mu\text{m}$ , indicating that the water in the size range of mudstone and fine sandstone is no longer driven out of the core sample after 7 MPa displacement pressure, the remaining water saturation in the sample is higher, and the water saturation of mudstone is higher than that of limestone and fine sandstone. The water saturation of Y1321-4 mudstone, medium-coarse grained sandstone and conglomerate basically no longer changes significantly when the methane flooding water pressure reaches about 9 MPa, and the water saturation distribution pore size range of these samples is large, the pore size is relatively large and there is a larger pore space. The water is no longer driven out of the core sample after 9 MPa displacement pressure. The remaining water saturation in the sample is low, and the water saturation of conglomerate is lower than that of medium-coarse grained sandstone. It can be seen that the larger the particle size of the rock after saturation, the greater the filling pressure required for the sample, and the lower the final residual water saturation, the more conducive to natural gas storage and migration. The higher the water saturation in the pores of the sample under the maximum methane flooding pressure (15 MPa), the less the movable the water content in the sample, the higher the bound water content, the lower the gas saturation in the actual underground reservoir and the lower the natural gas content in the rock reservoir after natural gas migration and filling. As shown in Figure 9, the gas saturation of different types of tight reservoirs is obviously different. The gas saturation of conglomerate is the highest (average of 65.84%), followed by limestone and sandstone (average of 41.59% and 42.21%, respectively). The coarser the grain size of sandstone, the higher the gas saturation and the lower the gas saturation of mudstone (except Y1321-4) (average of 27.64%).

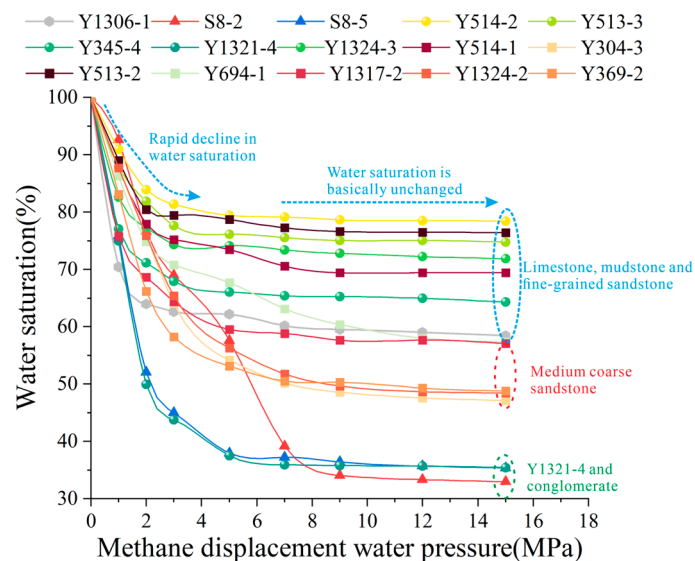


**Figure 9.** The change of water saturation with methane flooding pressure.

## 6. Main Controlling Factors of Gas–Water Distribution in Pores

The rock types of this experiment are diverse, including mudstone, limestone, sandstone and conglomerate with different particle sizes. The mineral and pore structure characteristics of different types of rock reservoirs are quite different, which has an important influence on the dynamic change characteristics of water molecule adsorption and gas–water distribution in rock reservoirs.

### 6.1. Organic Matter

The TOC content of mudstone samples is negatively correlated with the measured water vapor-adsorption capacity, the maximum adsorption capacity of a single molecular layer, water saturation and nuclear magnetic porosity (Figure 10a–c) and positively correlated with

gas saturation, indicating that with the increase in TOC content, the adsorption capacity of water molecules in mudstone samples and the occurrence of water under the maximum displacement pressure show a decreasing trend. Under certain filling pressure, water is more likely to be driven out of rock reservoirs, which is conducive to natural gas migration and accumulation. Previous studies have shown that TOC is positively correlated with the adsorption amount of water molecules, mainly due to the relatively low organic matter content of mudstone in this study, and the higher clay mineral content, which has a stronger control effect on the occurrence of water molecules, and the organic matter has a certain hydrophobicity [60]. With the increase in TOC content, water molecules occur with more and more difficulty in organic matter. There is no obvious development of organic matter pores in the mudstone samples, and there is no pore space for water supply molecules formed by organic matter. The nuclear magnetic porosity obtained based on the nuclear magnetic resonance methane flooding experiment mainly characterizes the pore space of water molecules, so the increase in organic matter content is not conducive to the occurrence of water molecules. In addition, with the progress of water vapor adsorption, the water molecules that have been adsorbed on the pore surface will cover the pore wall with adsorption capacity, which will reduce its adsorption capacity, so that the maximum adsorption capacity of the monolayer decreases with the increase in TOC content. The correlation between  $R_o$  and water molecule-adsorption capacity of the five mudstone samples in this experiment is not strong, but it is inversely proportional to nuclear magnetic porosity and proportional to gas saturation (Figure 10d–f). The  $R_o$  of the mudstone sample is more than 2.0%, which is in the over-mature stage, and the organic matter type is type III. With the increase in the maturity of the organic matter, the higher oxygen/carbon atom ratio and the number of polar functional groups that are conducive to the adsorption of water molecules gradually decrease, and a large amount of aromatic carbon is not conducive to the adsorption of water molecules.

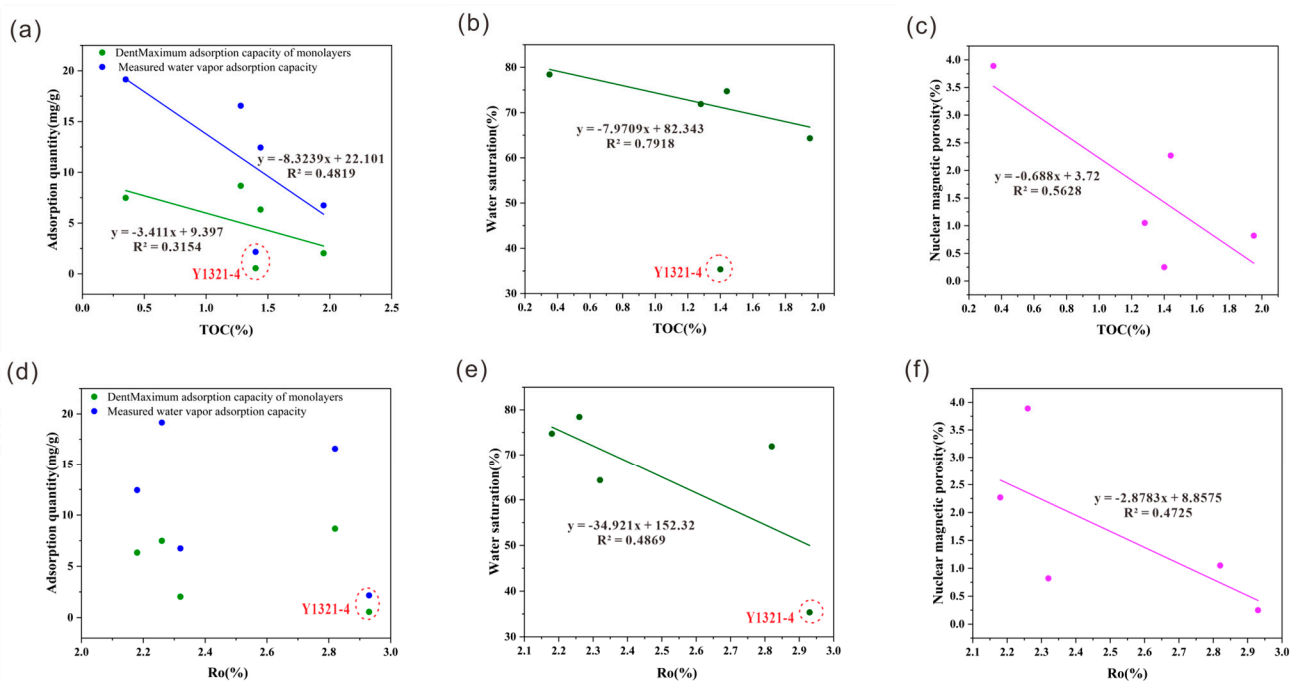


**Figure 10.** Effect of organic matter on gas–water distribution in pores. (a) The relationship between TOC content and mudstone water vapor adsorption capacity and Dent maximum adsorption capacity. (b) The relationship between TOC content and mudstone water saturation. (c) The relationship between TOC content and nuclear magnetic porosity of mudstone. (d) The relationship between  $R_o$  content and mudstone water vapor adsorption capacity and Dent maximum adsorption capacity. (e) The relationship between  $R_o$  content and mudstone water saturation (f) The relationship between  $R_o$  content and nuclear magnetic porosity of mudstone.



## 6.2. Inorganic Minerals

The clay mineral content of the experimental samples is positively correlated with the water vapor-adsorption capacity, the maximum adsorption capacity of the monolayer and the water saturation (Figure 11a,b), and negatively correlated with the gas saturation. This shows that with the increase in clay mineral content, the adsorption amount of water molecules in rock samples and the occurrence amount of water under the maximum displacement pressure show an increasing trend. The water in pores is not easily driven out of rock reservoirs, which is not conducive to natural gas migration and accumulation. Clay minerals are porous adsorption carriers with large specific surface area and pore structure. The adsorption sites in the pores are usually primary adsorption sites with strong hydrophilicity [61,62]. The clay minerals in the rock form different types of pores during the process of sedimentary compaction. The adsorption of water molecules in the pores is affected by van der Waals force, hydrogen bonding between water molecules and electrostatic force [63,64]; the layered structure of clay minerals may provide more surface area and microscopic pores for water vapor adsorption, which increases the adsorption capacity of water vapor. For small-scale interlayer pores, water molecules are inserted into the crystal layer in a molecular state. These water molecules embedded in the crystal layer will increase the spacing between the mineral layers, causing the clay minerals to expand and deform [65], further increasing the adsorption capacity of water molecules. Therefore, the increase in clay mineral content is not conducive to the occurrence and migration of natural gas. The relationship between clay minerals and NMR porosity is not obvious (Figure 11c), indicating that the occurrence space of water molecules is affected by many factors.

The quartz content of the experimental samples is negatively correlated with the water vapor-adsorption capacity, the maximum adsorption capacity of the monolayer and the water saturation (except Y1321-4), and positively correlated with the gas saturation (Figure 11d,e). This shows that with the increase in quartz content, the adsorption capacity of water molecules in the rock and the occurrence of water under the maximum displacement pressure show a decreasing trend. The water in the pores is more likely to be driven out of the rock pores, which is conducive to the occurrence and migration of natural gas in the reservoir. Quartz is generally considered to be a hydrophilic mineral, but after a series of complex geological processes, it may affect the hydrophilicity of the quartz surface. Combined with NMR gas flooding experiments, it is shown that the hydrophilicity of quartz almost disappears. Based on the comprehensive analysis of the information in the figure, the adsorption capacity of quartz content to water molecules is affected by various complex factors, resulting in an inverse correlation between quartz content and adsorption capacity. Quartz can be used as a skeleton to support pores, but with the increase in quartz content, it may block existing pores and reduce rock porosity. The relationship between quartz content and nuclear magnetic porosity is not clear, but there is an increasing trend (Figure 11f), indicating that quartz may be used as a skeleton to support rock pores. In summary, in the complex multi-component system of tight sandstone, quartz minerals mainly provide channels for natural gas migration.

The carbonate mineral content of the experimental samples is negatively correlated with the adsorption amount of water molecules in the rock, the adsorption amount of single molecular layer and the nuclear magnetic porosity (Figure 11g,i), indicating that with the increase in carbonate minerals, the adsorption amount of water molecules in the rock decreases; with the increase in displacement pressure, the water saturation tends to decrease, and the gas saturation tends to increase. The occurrence space of water molecules becomes smaller, so the increase in carbonate mineral content is conducive to natural gas accumulation. Studies have shown that the presence of calcite will inhibit the adsorption of water molecules by rocks [66]. As a kind of carbonate minerals, calcite is as high as 40.9% in Y345-4, and the porosity of two high carbonate minerals is 0.42% and 0.48%, respectively. Excessive carbonate mineral content may lead to reduced porosity of rocks and poor pore development, affecting the adsorption of water vapor, which is conducive to

the occurrence of natural gas. The composition of Y1306-1 is mainly carbonate minerals. Due to the non-hydrophilicity of carbonate minerals, the rock pores composed of them are large enough and the amount of water vapor adsorption will not be large, which is conducive to the migration and occurrence of natural gas. The content of carbonate minerals in tight sandstone is small. Because the small content of carbonate minerals can support the whole rock and increase the tiny pores of the rock, the porosity of 10 sandstone samples is much larger than that of mudstone, indicating that the increase in carbonate mineral content has a positive effect on the migration of natural gas for tight sandstone.

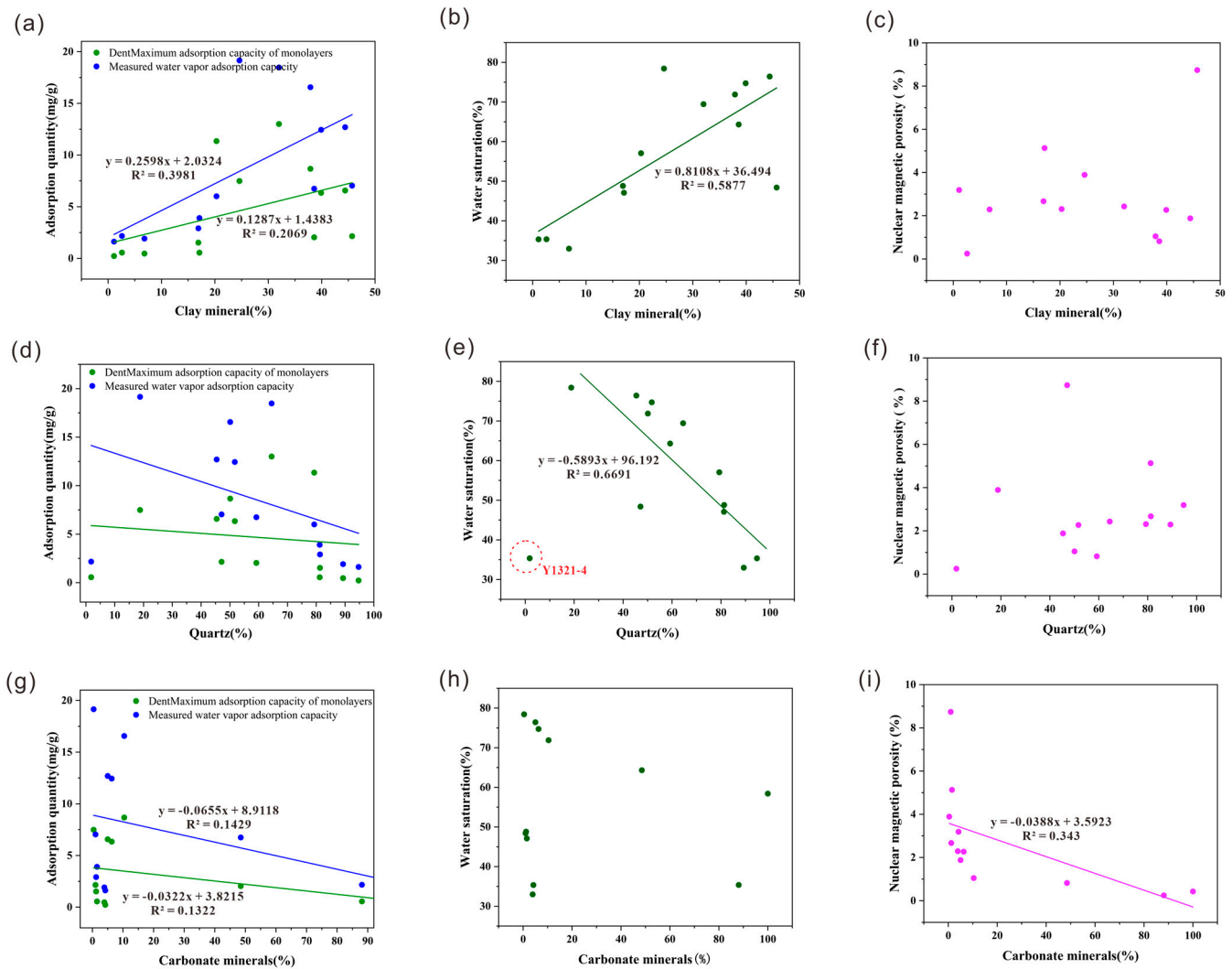


**Figure 11.** Effect of inorganic minerals on gas–water distribution in pores. (a) The relationship between clay mineral content and water vapor adsorption capacity and Dent maximum adsorption capacity of rock samples in Yan’an gas field. (b) The relationship between clay minerals and rock water saturation in Yan’an gas field. (c) The relationship between clay minerals and nuclear magnetic porosity of rocks in Yan’an gas field. (d) The relationship between quartz mineral content and water vapor adsorption capacity and Dent maximum adsorption capacity of rock samples in Yan’an gas field. (e) The relationship between  $R_0$  content and rock water saturation in Yan’an gas field. (f) The relationship between  $R_0$  content and nuclear magnetic porosity of rocks in Yan’an gas field. (g) The relationship between carbonate mineral content and water vapor adsorption capacity and Dent maximum adsorption capacity of rock samples in Yan’an gas field. (h) The relationship between carbonate minerals and rock water saturation in Yan’an gas field. (i) The relationship between carbonate minerals and nuclear magnetic porosity of rocks in Yan’an gas field.

### 6.3. Pore

Pores are the carriers of water vapor and gas in rocks, so it is of great significance to understand the adsorption of water molecules by pore structure for rock accumulation. The mesoporous specific surface area of the experimental samples is positively correlated with the water vapor-adsorption capacity, the maximum adsorption capacity of the monolayer and the water saturation (Figure 12a,b), and the relationship with the nuclear magnetic porosity is not clear (Figure 12c). This shows that with the increase in mesoporous specific surface area, the amount of water vapor adsorption in the rock sample and the amount of water storage under the maximum displacement pressure have an increasing trend, and the water molecules have no tendency to discharge the rock pores under a certain filling pressure, which is not conducive to the migration and accumulation of natural gas. The larger specific surface area provides more adsorption space and more adsorption sites for water vapor, which is of positive significance for the increase in water vapor adsorption. For the tight sandstone samples of Yan'an gas field (except Y1306-1), the organic matter content is low, and the sum of clay minerals and quartz accounts for more than 88%, and most of them are more than 90%. Both are hydrophilic inorganic minerals, so the pore space surface constructed by these two minerals is mostly hydrophilic. With the increase in mesoporous specific surface area, more water molecule-adsorption sites are provided.

The total mesoporous volume of the experimental samples is positively correlated with the water vapor-adsorption capacity, the maximum adsorption capacity of the monolayer and the water saturation (Figure 12d,e), and the relationship with the nuclear magnetic porosity is not clear (Figure 12f). The total pore volume of macropores is negatively correlated with water vapor-adsorption capacity, maximum adsorption capacity of monolayer and water saturation (Figure 12g,h), and positively correlated with NMR porosity (Figure 12i). This shows that for the mesoporous scale samples, with the increase in the total pore volume of the pores, the amount of water vapor adsorption and the amount of water storage under the maximum displacement pressure tend to increase. Under the action of a certain filling pressure, the water molecules do not have the tendency to discharge from the pores of the rock, which is more conducive to the occurrence of water molecules. For the macropore scale samples, with the increase in the total pore volume of the pores, the amount of water vapor adsorption and the amount of water storage under the maximum displacement pressure show a decreasing trend. The trend of water molecules to discharge the large pores of the rock under a certain filling pressure does not become larger, which is not conducive to the occurrence of water molecules and is more conducive to the migration and accumulation of natural gas. Under the action of van der Waals force, electrostatic force and hydrogen bond, water molecules will be adsorbed on the hydrophilic pore wall in the form of monolayer, and then gradually accumulate to form a thin layer of bound water film under the action of hydrogen bond and begin to carry out multi-layer adsorption to form cluster 'water droplets'. For mesoporous pores, larger pore volume provides more space for water molecules and more adsorption sites for this series of processes, which is a powerful factor for the increase in water vapor adsorption, so it is not conducive to the occurrence of natural gas. The pore volume of the sample is mainly composed of intergranular pores, intragranular pores and organic pores between inorganic minerals, and the pore volume constructed by inorganic minerals is the main pore. For macropores, the pore space in the rock is large enough, and the pore sites required for water molecule adsorption do not completely occupy the adsorption sites of macropores after reaching a certain extent. The permeability and porosity of macropores are also larger than those of mesopores, which provides a larger pore volume for the migration and occurrence of gas in rocks, which is conducive to natural gas accumulation. In summary, for tight sandstone, the adsorption of water molecules in pore volume is mainly controlled by weak hydrogen bonds and van der Waals forces. For the increase in mesoporous pore volume, it is not conducive to the migration and occurrence of natural gas in rock pores. With the increase in macropore pore volume, it is beneficial to the migration and occurrence of natural gas in rock pores, indicating that larger pores are more conducive to tight sandstone gas accumulation.

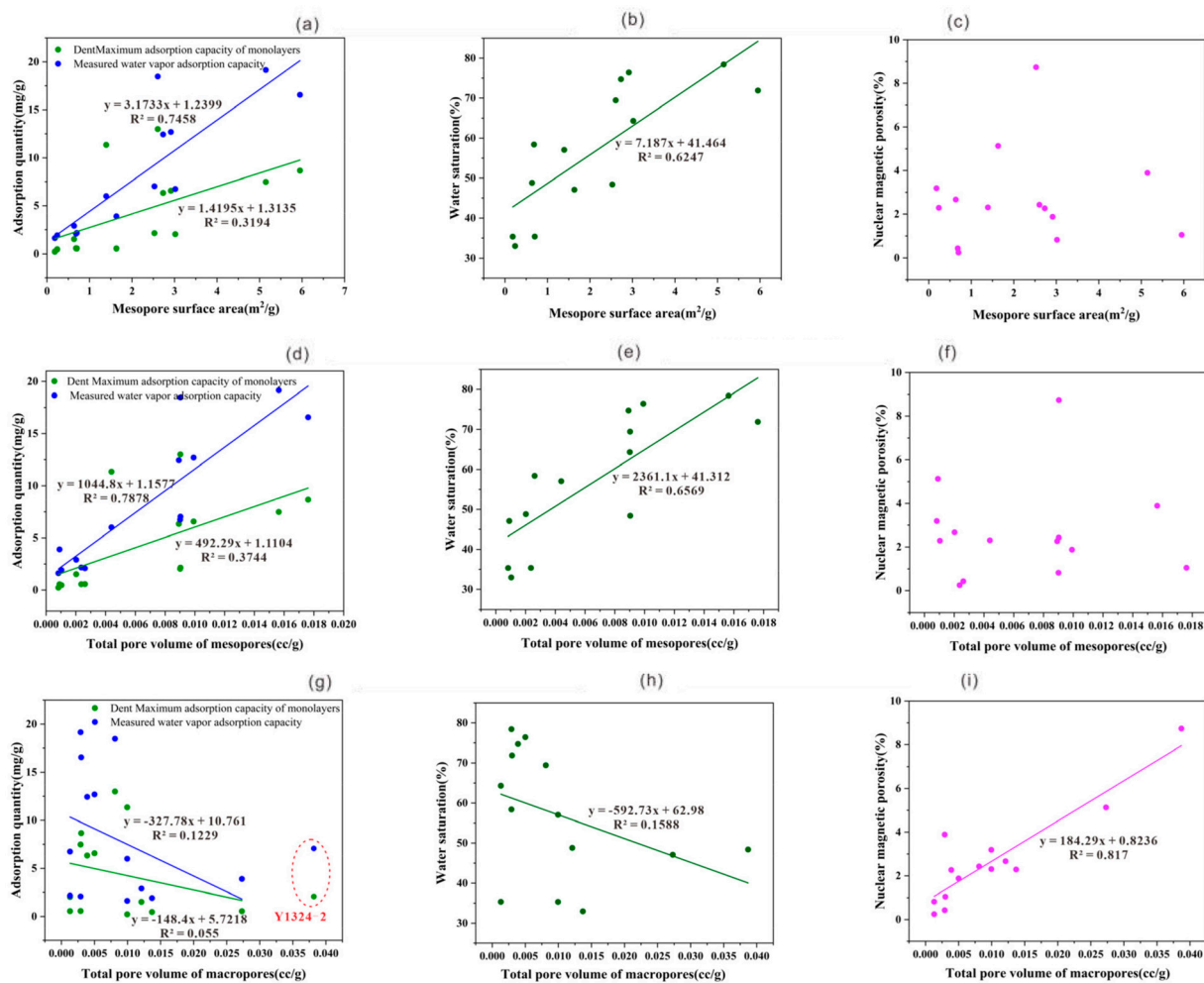


**Figure 12.** Effect of pore structure on gas–water distribution in pores. (a) The relationship between mesopore surface area and water vapor adsorption capacity and Dent maximum adsorption capacity of rock samples in Yan’an gas field. (b) The relationship between mesopore surface area and rock water saturation in Yan’an gas field. (c) The relationship between mesopore surface area and nuclear magnetic porosity of rocks in Yan’an gas field. (d) The relationship between total pore volume of mesopores and water vapor adsorption capacity and Dent maximum adsorption capacity of rock samples in Yan’an gas field. (e) The relationship between total pore volume of mesopores and rock water saturation in Yan’an gas field. (f) The relationship between total pore volume of mesopores and nuclear magnetic porosity of rocks in Yan’an gas field. (g) The relationship between total pore volume of macropores and water vapor adsorption capacity and Dent maximum adsorption capacity of rock samples in Yan’an gas field. (h) The relationship between total pore volume of macropores and rock water saturation in Yan’an gas field. (i) The relationship between total pore volume of macropores and nuclear magnetic porosity of rocks in Yan’an gas field.

## 7. Conclusions

In this paper, 15 tight reservoir rock samples in Yan’an gas field are taken as the research object. The characteristics and influencing factors of gas and water changes in the pores are addressed with the water vapor-adsorption test and nuclear magnetic resonance methane flooding test. The main achievements are as follows:

(1) The isothermal adsorption curve of water molecules in tight reservoir rock samples of Yan’an gas field conforms to type II. The hysteresis loops of rock samples are mainly H2-H3 type, H3 type and H3-H4 type. The samples develop flat slit structure, cracks, narrow fracture pores and ink bottle-shaped pores. Water molecules mainly occur in clay minerals and the fracture-type and parallel plate-like pores that are mainly involved in the



formation. The Dent model is the best model to characterize the adsorption behavior of water vapor in tight rock reservoirs.

(2) The variation characteristics of water content and gas saturation of different types of tight reservoir rock samples in Yan'an gas field are quite different. The dynamic change characteristics of gas and water in large-sized pores are obvious, while the dynamic change characteristics of gas and water in rocks with small pore size are not obvious, and the gas saturation is low, which is not conducive to the occurrence and migration of natural gas.

(3) The development of organic matter in tight reservoir mudstone is not conducive to the occurrence of water molecules, which is conducive to gas adsorption. Clay minerals and smaller pores are the main reasons for the high water saturation of different types of tight reservoir rocks. Quartz and carbonate minerals play a positive role in the occurrence of natural gas. The larger the pore size, the more favorable the rock reservoir is to the migration and occurrence of natural gas, which is helpful to the accumulation of tight sandstone gas.

**Author Contributions:** Methodology, Y.W. (Yongping Wan) and Z.W.; Formal analysis, Y.W. (Yongping Wan), M.W., X.M. and J.H.; Data curation, Y.W. (Yongping Wan), Z.W., M.W., J.H., M.H. and Y.W. (Ye Wang); Writing—original draft, Y.W. (Yongping Wan), Z.W. and X.M.; Writing—review & editing, Y.W. (Yongping Wan) and M.W.; Supervision, K.L.; Project administration, K.L.; Funding acquisition, S.H. All authors have read and agreed to the published version of the manuscript.

**Funding:** This research was funded by the Fundamental Research Funds for the Central Universities grant number 2023ZKPYDC07. The editors and anonymous reviewers are gratefully acknowledged.

**Data Availability Statement:** Data are contained within the article.

**Conflicts of Interest:** Authors Yongping Wan, Zhenchuan Wang and Meng Wang were employed by the company Gasfield Company of Shaanxi Yanchang Petroleum Group Co., Ltd. The remaining authors declare that the research was conducted in the absence of any commercial or financial relationships that could be construed as a potential conflict of interest.

## References

- Li, Q.; Wang, Y.L.; Wang, F.L.; Wu, J.P.; Tahir, M.U.; Li, Q.C.; Yuan, L.; Liu, Z.H. Effect of thickener and reservoir parameters on the filtration property of CO<sub>2</sub> fracturing fluid. *Energy Source Part A Recovery Util. Environ. Eff.* **2019**, *42*, 1705–1715. [[CrossRef](#)]
- Wang, X.X.; Mei, L.F.; Quan, Y.W. Types of tight sand gas accumulation and its exploration prospect. *Nat. Gas Geosci.* **2007**, *18*, 351–355.
- Law, B.E. Basin-centered gas system. *AAPG Bull.* **2002**, *86*, 1891–1919.
- Zhu, H.Y.; Xu, X.; An, L.Z.; Guo, C.M.; Xiao, J.R. An experimental on occurrence and mobility of pore water in tight gas reservoirs. *Pet. Sci.* **2016**, *37*, 230–236.
- Xie, Z.Y.; Yang, C.L.; Li, J.; Jin, H.; Wang, X.J.; Hao, C.G.; Zhang, L.; Guo, J.Y. Charging simulation experiment and characteristics of tight sandstone gas reservoirs: A case study of the Upper Triassic Xujiahe Formation sandstone gas reservoir in the central Sichuan Basin. *Nat. Gas Ind.* **2020**, *40*, 31–40.
- Xu, X.; Hu, Y.; Shao, L.Y.; Wang, J.P.; Chen, Y.L.; Jiao, C.Y. Experimental simulation of gas accumulation mechanism in sandstone reservoir: A case study of Sulige gas field, Ordos basin. *J. China Univ. Min. Technol.* **2017**, *46*, 1323–1331+1339.
- Wang, X.Z. Advances and prospects in oil and gas exploration and development of Shanxi Yanchang Petroleum(Group) Co., Ltd. *China Pet. Explor.* **2018**, *23*, 36–43.
- Chen, C.B.; Yang, Y.Y.; Shao, J.H.; Zhu, Y.S.; Chen, X.J.; Shi, L.; Meng, D. Origin and distribution of formation water in tight sandstone reservoirs in the northeastern Ordos Basin. *Oil Gas Geol.* **2019**, *40*, 313–325.
- Hu, P.; Yu, X.H.; Wang, J.; Zhou, J.S.; Han, X.Q.; Li, Y.L.; Shi, X.; Xu, L.Q.; Fang, D.K.; Chen, H.L. Chemical characteristics of Benxi Formation water and its significance for natural gas accumulation in Southeast Ordos Basin. *J. Northwest Univ. Nat. Sci. Ed.* **2017**, *47*, 92–100+109.
- Ma, H.Y.; Zhou, L.F.; Deng, X.Q.; Li, J.H.; Yang, L.P. The chemical characteristics and geological significance of formation water of chana 8 Subsection in Jiyuan area of Ordos Basin. *J. Northwest Univ. Nat. Sci. Ed.* **2013**, *43*, 253–257.
- Wang, X.M.; Zhao, J.Z.; Liu, X.S.; Fan, L.Y. Distribution of formation water in tight sandstone reservoirs of western Sulige gas field, Ordos Basin. *Oil Gas Geol.* **2012**, *33*, 802–810.
- Li, Q.C.; Liu, J.; Wang, S.M.; Guo, Y.; Han, X.Y.; Li, Q.; Cheng, Y.F.; Dong, Z.; Li, X.Z.; Zhang, X.D. Numerical insights into factors affecting collapse behavior of horizontal wellbore in clayey silt hydrate-bearing sediments and the accompanying control strategy. *Ocean Eng.* **2024**, *297*, 117029. [[CrossRef](#)]

13. Lu, T. Evaluation of Gas-Water Relationship of Tight Sandstones in the Upper Paleozoic, Dingbei Area, Ordos Basin. Master's Thesis, Chengdu University of Technology, Chengdu, China, 2020.
14. Xu, S.; Zhu, Y.S.; Li, X.Y.; Fan, Z.Q. Cause analysis of gas-water inversion in Zizhou gas field. *Ground Water* **2013**, *35*, 13–15.
15. Zhang, X.X.; Zhao, J.Z.; Ma, J.H.; Zhang, J. Ancient and modern tectonic characteristics of 8th member of Xiashihezi Formation in Sulige Gasfield, Ordos Basin, China and their control effects on gas-water distribution. *J. Xi'an Shiyou Univ. (Nat. Sci. Ed.)* **2011**, *26*, 14–20.
16. Li, Z.D.; Hao, S.M.; Li, L.; Hui, K.Y.; Guo, M. Comparison between the Upper Paleozoic gas reservoirs in Ordos Basin and deep basin gas reservoirs. *Oil Gas Geol.* **2009**, *30*, 149–155.
17. Cong, P.; Zhao, J.X.; Wei, W.; Meng, L.J.; Li, P.J.; Li, J.; Zhang, Y.C.; Wei, S.Y.; Peng, S.J. Gas and water distribution patterns in low maturity gas areas of coal bearing tight sandstone Taking the Taiyuan Formation in the northeast of the Yishan Slope of the Ordos Basin as an example. *J. Miner. Petrol.* **2024**; *Final Recruitment*.
18. Meng, D.W.; Jia, A.L.; Ji, G.; He, D.B. Water and gas distribution and its controlling factors of large scale tight sand gas: A case study of western Sulige gas field, Ordos Basin, Nw China. *Pet. Explor. Dev.* **2016**, *43*, 607–614. [[CrossRef](#)]
19. Zhao, S.; Yong, Z.Q. Gas-water distribution and genesis of the tight sandstone gas field in Member 4 of Xujiahe Formation in Chongxi of Central Sichuan, China. *J. Chengdu Univ. Technol. Sci. Technol. Ed.* **2012**, *39*, 164–169.
20. Zhou, X.; Jiang, Y.; Chen, L.; Lei, X.; Xiong, Z.; Yang, B. Study on water production mechanism and seepage law of tight sandstone gas reservoirs in Suxi. *Petrochem. Ind. Appl.* **2016**, *35*, 76–83.
21. Zhao, Z.D.; Qiao, X.Y.; Zhou, J.S.; Cao, B.F.; Yin, J.T.; Xu, Y.L.; Cao, J.; Yang, X. The densification of sandstone reservoir and its coupling relationship with hydrocarbon charging and accumulation: A case study of the Upper Paleozoic in Yan'an Gas Field, Ordos Basin. *Fault-Block Oil Gas Field* **2023**, *30*, 363–371.
22. Zhao, Q.P.; Wang, R.G.; Gao, F.; Yin, X. Provenance analysis of Upper Paleozoic in Yanchang Blocks, the Southeast Ordos Basin. *J. Northwest Univ. Nat. Sci. Ed.* **2015**, *45*, 933–941.
23. Zhou, J.S.; Wang, N.X.; Zhao, Q.P.; Lin, G.F.; Yin, X.; Gao, F.; Wei, H.; Han, X.Q. Analysis on Controlling Factors and Sandstone Reservoir Characteristics of the Upper Paleozoic in Ordos Basin. *J. Jiangnan Pet. Inst.* **2014**, *36*, 27–33+5.
24. Wang, X.Z.; Qiao, X.Y.; Zhang, L.; Wang, Y.K.; Zhou, J.S.; Du, Y.H.; Cao, J.; Xin, C.P.; Song, J.X.; Yuan, F.Z. Innovation and scale practice of key technologies for the exploration and development of tight sandstone gas reservoirs in Yan'an Gas Field of southeastern Ordos Basin. *Nat. Gas Ind.* **2022**, *42*, 102–113.
25. Sun, J.B.; Liu, G.; Shi, P.; Xue, P.; Liu, C.; Xu, J. Reservoir characteristics and analysis of shale gas resource potential in Shanxi Formation in Yan'an Area. *Unconv. Oil Gas* **2023**, *10*, 44–51.
26. Lei, K.Y.; Gao, X.P.; Li, Y.; Ma, Y.G.; Lv, M.; Liu, Y.Y. The study focuses on the well control scale of the Upper Paleozoic tight sandstone gas reservoir in Yan'an Gas Field. *Petrochem. Ind. Technol.* **2024**, *31*, 242–244.
27. Wang, R.G.; Zhou, J.S.; Du, Y.H.; Li, W.H. Deposition evolution model of the Carboniferous-Permian in Yan'an gas field, the southeastern Ordos Basin. *Geol. Sci.* **2021**, *56*, 1088–1105.
28. Yu, X.H.; Wang, X.Z.; Wang, N.X.; Shan, X.; Zhou, J.S.; Han, X.Q.; Li, Y.L.; Du, Y.H.; Zhao, C.F. Sequence stratigraphic framework and sedimentary evolution characteristics of gas-bearing sandbody in the Upper Paleozoic in southeastern Ordos Basin. *J. Palaeogeogr.* **2017**, *19*, 935–954.
29. Langmuir, I. The adsorption of gases on plane surfaces of glass, mica and platinum. *J. Chem. Phys.* **2015**, *40*, 1361–1403. [[CrossRef](#)]
30. Freundlich, H. Über die Adsorption in Lösungen. *Z. Phys. Chem.* **1907**, *57U*, 385–470. [[CrossRef](#)]
31. Halsey, G. Physical Adsorption on Non-Uniform Surfaces. *J. Chem. Phys.* **1948**, *16*, 931–937. [[CrossRef](#)]
32. Johansen, R.T.; Dunning, H.N. Water-vapor adsorption on clays. *Clay Clay Miner.* **1957**, *6*, 249–258. [[CrossRef](#)]
33. Dubinin, M.M.; Serpinsky, V.V. Isotherm equation for water vapor adsorption by microporous carbonaceous adsorbents. *Carbon* **1981**, *19*, 402–403. [[CrossRef](#)]
34. Strydom, C.A.; Campbell, Q.P.; Roux, M.L.; Preez, S.M. Validation of Using a Modified BET Model to Predict the Moisture Adsorption Behavior of Bituminous Coal. *Int. J. Coal Prep. Util.* **2016**, *36*, 28–43. [[CrossRef](#)]
35. D'Arcy, R.L.; Watt, I.C. Analysis of sorption isotherms of non-homogeneous sorbents. *Trans. Faraday Soc.* **1970**, *66*, 1236–1245. [[CrossRef](#)]
36. Anderson, R.B. Modifications of the Brunauer, Emmett and Teller equation. *J. Am. Chem. Soc.* **1946**, *68*, 686–691. [[CrossRef](#)]
37. De, B.J.H. *The Dynamical Character of Adsorption*; Clarendon Press: Oxford, UK, 1953.
38. Guggenheim, E.A. *Applications of Statistical Mechanics*; Clarendon Press: Oxford, UK, 1966.
39. GB/T 19145-2022; Determination for Total Organic Carbon in Sedimentary Rock. China National Standards: Beijing, China, 2022.
40. GB/T 18602-2012; Rock pyrolysis Analysis. China National Standards: Beijing, China, 2012.
41. SY/T 5163-2018; Analysis Method for Clay Minerals and Ordinary Non-Clay Minerals in Sedimentary Rocks by the X-ray Diffraction. China National Standards: Beijing, China, 2018.
42. GB/T 21650.2-2008/ISO 15901-2:2006; Pore Size Distribution and Porosity of Solid Materials by Mercury Porosimetry and Gas Adsorption. Part 2: Analysis of Mesopores and Macropores by Gas Adsorption. China National Standards: Beijing, China, 2008.
43. GB/T 21650.3-2011/ISO 15901-3:2007; Pore Size Distribution and Porosity of Solid Materials by Mercury Porosimetry and Gas Adsorption. Part 3: Analysis of Micropores by Gas Adsorption. China National Standards: Beijing, China, 2011.
44. GB/T 21650.1-2008/ISO 15901-1:2005; Pore Size Distribution and Porosity of Solid Materials by Mercury Porosimetry and Gas Adsorption. Part 1: Mercury Porosimetry. China National Standards: Beijing, China, 2008.

45. Thommes, M.; Kaneko, K.; Neimark, A.V.; Olivier, J.M.; Reinoso, F.R.; Rouquerol, J.; Sing, K.S. Physisorption of gases, with special reference to the evaluation of surface area and pore size distribution (IUPAC Technical Report). *Pure Appl. Chem.* **2015**, *87*, 1051–1069. [[CrossRef](#)]
46. Rouquerol, F.; Rouquerol, J.; Sing, K.S.W. *Adsorption by Powders and Porous Solids: Principles, Methodology and Applications*; Elsevier Science: London, UK, 1998; p. 135510063.
47. Zhang, Y.; Hui, D.; Zhang, J.; Zhang, D.L.; Jiang, R. Characteristics and main controlling factors of water vapor adsorption in marine shale: A case study of the Lower Silurian Longmaxi shales in southern Sichuan Basin. *Oil Gas Geol.* **2022**, *43*, 1431–1444.
48. Everett, D.H.; Powl, J.C. Adsorption in slit-like and cylindrical micropores in the Henry's law region. A model for the microporosity of carbons. *J. Chem. Soc. Faraday Trans.* **1976**, *72*, 619–636. [[CrossRef](#)]
49. Mahajan, O.P.; Walker, P.L. Water adsorption on coals. *Fuel* **1971**, *50*, 308–317. [[CrossRef](#)]
50. Charriere, D.; Behra, P. Water sorption on coals. *J. Colloid Interface Sci.* **2010**, *344*, 460–467. [[CrossRef](#)] [[PubMed](#)]
51. Mccutcheon, A.L. Kinetics of water adsorption/desorption on bituminous coals. *Energy Fuels* **2001**, *43*, 233. [[CrossRef](#)]
52. Mccutcheon, A.L.; Barton, W.A. Contribution of Mineral Matter to Water Associated with Bituminous Coals. *Energy Fuels* **1999**, *13*, 160–165. [[CrossRef](#)]
53. Furmaniak, S.; Gauden, P.A.; Terzyk, A.P.; Rychlicki, G. Water adsorption on carbons-critical review of the most popular analytical approaches. *Adv. Colloid Interface Sci.* **2008**, *137*, 82–143. [[CrossRef](#)] [[PubMed](#)]
54. Li, J.; Li, X.F.; Wang, X.Z.; Li, Y.Y.; Wu, K.L.; Shi, J.T.; Yang, L.; Feng, D.; Zhang, T.; Yu, P.L. Water distribution characteristic and effect on methane adsorption capacity in shale clay. *Int. J. Coal Geol.* **2016**, *159*, 135–154. [[CrossRef](#)]
55. Dubinin, M.M.; Serpinsky, V.V. Water vapour adsorption on microporous activated carbons. *Carbon R. Acad. Sci. URSS* **1981**, *285*, 1151–1157.
56. Sang, G.J.; Liu, S.M.; Elsworth, D. Water vapor sorption properties of Illinois shales under dynamic water vapor conditions: Experimentation and modeling. *Water Resour. Res.* **2019**, *55*, 7212–7228. [[CrossRef](#)]
57. Yang, Y.P.; Chen, M.Y.; Tian, F.C.; Wang, Z.Y.; Tian, S.O.; Fang, R.Y. Research on differences of adsorbed water characteristics of low rank and high rank coals based on water vapor adsorption model. *Saf. Coal Mines* **2021**, *52*, 7–12.
58. Duan, S.; Geng, L.K.; Li, G.D.; Ling, X.Y. Water vapour adsorption isotherms of shales: Thermodynamic properties and microstructure. *Fluid Phase Equilib.* **2023**, *563*, 113583. [[CrossRef](#)]
59. Dang, W.; Jiang, S.; Zhang, J.C.; Li, P.; Nie, H.K.; Liu, Y.; Li, F.; Sun, J.T.; Tao, J.; Shan, C.A.; et al. A systematic experimental and modeling study of water adsorption/desorption behavior in organic-rich shale with different particle sizes. *Chem. Eng. J.* **2021**, *426*, 130596. [[CrossRef](#)]
60. Yu, L.J.; Liu, K.Y.; Fan, M.; Liu, Y.X. Co-occurring characteristics of pore gas and water in shales: A case study of the Lower Silurian Longmaxi Formation in the southeastern Sichuan Basin. *Exp. Pet. Geol.* **2021**, *43*, 1089–1096.
61. Feng, D.; Li, X.F.; Wang, X.Z.; Li, J.; Sun, F.R.; Sun, Z.; Zhang, T.; Li, P.H.; Chen, Y.; Zhang, X. Water adsorption and its impact on the pore structure characteristics of shale clay. *Appl. Clay Sci.* **2018**, *155*, 126–138. [[CrossRef](#)]
62. Kim, C.; Devegowda, D. Molecular dynamics study of fluid-fluid and solid-fluid interactions in mixed-wet shale pores. *Fuel* **2022**, *319*, 123587. [[CrossRef](#)]
63. Li, J.; Chen, Z.X.; Li, X.F.; Wang, X.A.; Wu, K.L.; Feng, D.; Qu, S.Y. A quantitative research of water distribution characteristics inside shale and clay nanopores. *Sci. Sin. Technol.* **2018**, *48*, 1219–1233. [[CrossRef](#)]
64. Passey, Q.R.; Bohacs, K.M.; Esch, W.L.; Klimentidis, R.; Sinha, S. From oil-prone source rock to gas-producing shale reservoir-geologic and petrophysical characterization of unconventional shale-gas reservoirs. In Proceedings of the SPE International Oil & Gas Conference and Exhibition, Beijing, China, 8–10 June 2010; p. 131350.
65. Zhang, Y.Y.; Chen, M.; Deng, Y.; Jin, Y. Molecular Dynamics Simulation of Temperature and Pressure Effects on Hydration Characteristics of Montmorillonites. *Acta Silic. Sin.* **2018**, *46*, 1489–1498.
66. Schultz, L.N.; Andersson, M.P.; Dalby, K.N.; Muter, D.; Okhrimenko, D.V.; Fordsmand, H.; Stipp, S.L.S. High surface area calcite. *J. Cryst.* **2013**, *371*, 34–38. [[CrossRef](#)]

**Disclaimer/Publisher's Note:** The statements, opinions and data contained in all publications are solely those of the individual author(s) and contributor(s) and not of MDPI and/or the editor(s). MDPI and/or the editor(s) disclaim responsibility for any injury to people or property resulting from any ideas, methods, instructions or products referred to in the content.